

Blind Image Deconvolution using Pretrained Generative Priors

Muhammad Asim*

Fahad Shamshad*

Ali Ahmed

{msee16001,fahad.shamshad,ali.ahmed}@itu.edu.pk

Department of Electrical Engineering,
Information Technology University,
Lahore, Pakistan

Abstract

This paper proposes a novel approach to regularize the *ill-posed* blind image deconvolution (blind image deblurring) problem using deep generative networks. We employ two separate deep generative models — one trained to produce sharp images while the other trained to generate blur kernels from lower-dimensional parameters. To deblur, we propose an alternating gradient descent scheme operating in the latent lower-dimensional space of each of the pretrained generative models. Our experiments show excellent deblurring results even under large blurs and heavy noise. To improve the performance on rich image datasets not *well learned* by the generative networks, we present a modification of the proposed scheme that governs the deblurring process under both generative and classical priors.

Introduction and Related Work

Blind image deblurring aims to recover a true image i and a blur kernel k from blurry and possibly noisy observation y . For a uniform and spatially invariant blur, it can be mathematically formulated as

$$y = i \otimes k + n, \quad (1)$$

where \otimes is a convolution operator and n is an additive Gaussian noise. In its full generality, the inverse problem (1) is severely ill-posed as many different instances of i , and k fit the observation y [5, 17].

To resolve between multiple instances, priors are introduced on images and/or blur kernels in the image deblurring algorithms. Priors assume an *a priori* model on the true image/blur kernel or both. These natural structures expect images or blur kernels to be sparse in some transform domain; see, for example, [4, 6, 8, 12, 19, 39]. Some of the other penalty functions to improve the conditioning of the blind image deblurring problem are low-rank [27], and total variation based priors [24]. A recently introduced dark channel prior [25] also shows promising results; it assumes a sparse structure on the dark channel of the image, and exploits this structure in an optimization program [34] to solve the blind image deblurring problem. Other works include extreme channel priors [36], outlier robust deblurring [7], learned data fitting [26], and discriminative prior based blind image deblurring approaches [20]. Although generic and applicable to multiple applications, these engineered models are not very effective as many unrealistic images also fit the prior model [10].

* The authors contributed equally.

© 2019. The copyright of this document resides with its authors.

It may be distributed unchanged freely in print or electronic forms.

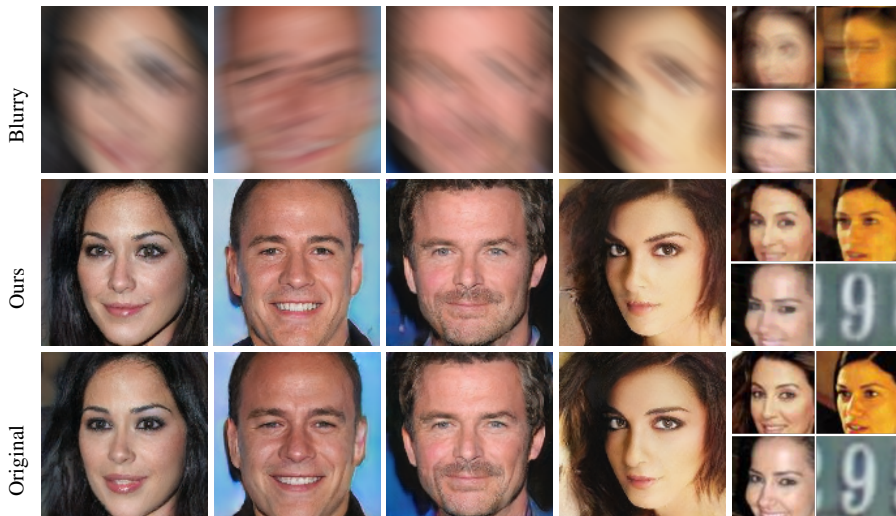


Figure 1: Blind image deblurring using deep generative priors.

Recently deep learning based blind image deblurring approaches have shown impressive results due to their power of learning from large training data [13, 18, 22, 23, 29, 35]. Generally, these deep learning based approaches invert the forward acquisition model of blind image deblurring via end-to-end training of deep neural networks in a supervised manner. The main drawback of this end-to-end deep learning approach is that it does not explicitly take into account the knowledge of forward map (1), but rather learns implicitly from training data. Consequently, the deblurring is more sensitive to changes in the blur kernels, images, or noise distributions in the test set that are not representative of the training data, and often requires expensive retraining of the network for a competitive performance [21].

Meanwhile, neural network based implicit generative models such as generative adversarial networks (GANs) [10] and variational autoencoders (VAEs) [16] have found much success in modeling complex data distributions especially that of images. Recently, GANs and VAEs have been used for blind image deblurring but only in an end-to end manner [18, 23, 35], which is completely different from our approach as will be discussed in detail. These methods show competitive performance, but since these generative model based approaches are end-to-end they suffer from the same draw backs as other deep learning based deblurring approaches. On the other hand, pretrained generative models have recently been employed as regularizers to solve inverse problems in imaging including compressed sensing [9, 30], image inpainting [37], Fourier ptychography [32], and phase retrieval [12, 31]. However the applicability of these pretrained generative models in blind image deblurring is relatively unexplored.

Recently [9] employ a combination of multiple untrained deep generative models and show their effectiveness on various image layer decomposition tasks including image water mark removal, image dehazing, image segmentation, and transparency separation in images and videos. Different from their approach, we show the effectiveness of our blind image deblurring method by leveraging trained generative models for images and blurs.

In this work, we use the expressive power of pretrained GANs and VAEs to tackle the challenging problem of blind image deblurring. Our experiments in Figure 1 confirm that

integrating deep generative priors in the image deblurring problem enables a far more effective regularization yielding sharper and visually appealing deblurred images. Specifically, our main contributions are

- To the best of our knowledge, this is the first instance of utilizing pretrained generative models for tackling challenging problem of blind image deblurring.
- We show that simple gradient descent approach assisted with generative priors is able to recover true image and blur kernel, to within the range of respective generative models, from blurry image.
- We investigate a modification of the loss function to allow the recovered image some leverage/slack to deviate from the range of the image generator. This modification effectively addresses the performance limitation due to the range of the generator.
- Our experiments demonstrate that our approach produce superior results when compared with traditional image priors and unlike deep learning based approaches does not require expensive retraining for different noise levels.

2 Problem Formulation and Proposed Solution

We assume the image $i \in \mathbb{R}^n$ and blur kernel $k \in \mathbb{R}^n$ in (1) are members of some structured classes \mathcal{I} of images, and \mathcal{K} of blurs, respectively. For example, \mathcal{I} may be a set of celebrity faces and \mathcal{K} comprises of motion blurs. A representative sample set from both classes \mathcal{I} and \mathcal{K} is employed to train a generative model for each class. We denote $G_{\mathcal{I}} : \mathbb{R}^l \rightarrow \mathbb{R}^n$ and $G_{\mathcal{K}} : \mathbb{R}^m \rightarrow \mathbb{R}^n$ as the generators for class \mathcal{I} , and \mathcal{K} , respectively. Given low-dimensional inputs $z_i \in \mathbb{R}^l$, and $z_k \in \mathbb{R}^m$, the pretrained generators $G_{\mathcal{I}}$ and $G_{\mathcal{K}}$ generate new samples $G_{\mathcal{I}}(z_i)$, and $G_{\mathcal{K}}(z_k)$ that are representative of the classes \mathcal{I} and \mathcal{K} , respectively. Once trained, the weights of the generators are fixed. To recover the sharp image and blur kernel (i, k) from the blurred image y in (1), we propose minimizing the following objective function

$$(\hat{i}, \hat{k}) := \underset{\substack{i \in \text{Range}(G_{\mathcal{I}}) \\ k \in \text{Range}(G_{\mathcal{K}})}}{\text{argmin}} \|y - i \otimes k\|^2, \quad (2)$$

where $\|\cdot\|$ is the ℓ_2 -distance, $\text{Range}(G_{\mathcal{I}})$ and $\text{Range}(G_{\mathcal{K}})$ is the set of all the images and blurs that can be generated by $G_{\mathcal{I}}$ and $G_{\mathcal{K}}$, respectively. In words, we want to find an image i and a blur kernel k in the range of their respective generators, that best explain the forward model (1). Ideally, the range of a pretrained generator comprises of only the samples drawn from the probability distribution of the training image or blur class. Constraining the solution (\hat{i}, \hat{k}) to lie only in generator ranges forces the solution to be the members of classes \mathcal{I} and \mathcal{K} .

The minimization program in (2) can be equivalently formulated in the lower dimensional, latent representation space as follows:

$$(\hat{z}_i, \hat{z}_k) = \underset{z_i \in \mathbb{R}^l, z_k \in \mathbb{R}^m}{\text{argmin}} \|y - G_{\mathcal{I}}(z_i) \otimes G_{\mathcal{K}}(z_k)\|^2. \quad (3)$$

This optimization program can be thought of as tweaking the latent representation vectors z_i and z_k , (input to the generators $G_{\mathcal{I}}$, and $G_{\mathcal{K}}$, respectively) until these generators generate an image i and blur kernel k whose convolution comes as close to y as possible. Incorporating

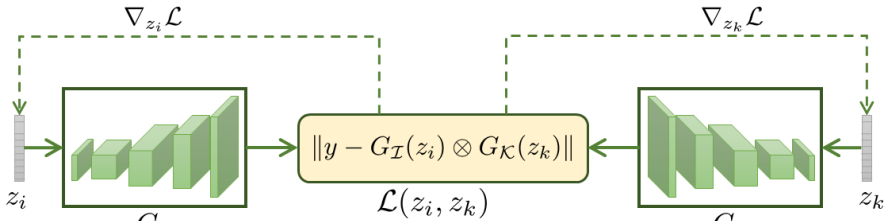


Figure 2: Block diagram of proposed approach. Low dimensional parameters z_i and z_k are updated to minimize the measurement loss using alternating gradient descent. The optimal pair (\hat{z}_i, \hat{z}_k) generate image and blur estimates $(G_{\mathcal{I}}(\hat{z}_i), G_{\mathcal{K}}(\hat{z}_k))$.

the fact that latent representation vectors z_i , and z_k are assumed to be coming from standard Gaussian distributions, we further augment the measurement loss in (3) with ℓ_2 penalty terms on the latent representations. The resultant optimization program is then

$$\operatorname{argmin}_{z_i \in \mathbb{R}^l, z_k \in \mathbb{R}^m} \|y - G_{\mathcal{I}}(z_i) \otimes G_{\mathcal{K}}(z_k)\|^2 + \gamma \|z_i\|^2 + \lambda \|z_k\|^2, \quad (4)$$

where γ and λ are free scalar parameters. For brevity, we denote the objective function above by $\mathcal{L}(z_i, z_k)$. Importantly, the weights of the generators are always fixed as they enter into this algorithm as pretrained models. To minimize this non-convex objective, we begin by initializing z_i and z_k by sampling from standard Gaussian distribution, and resort to an alternating gradient descent algorithm by taking a gradient step in one of these while fixing the other to find a minima (\hat{z}_i, \hat{z}_k) . To avoid being stuck in a not good enough local minima, we restart the algorithm with a new random initialization (Random Restarts) when the measurement loss in (3) does not reduce sufficiently after reasonably many iterations. We dubbed proposed deblurring algorithm as *Deep Deblur* and denote blurry image deblurred via *Deep Deblur* as \hat{i}_{DD} . The estimated deblurred image and the blur kernel are acquired by a forward pass of the solutions \hat{z}_i and \hat{z}_k through the generators $G_{\mathcal{I}}$ and $G_{\mathcal{K}}$. Mathematically, $(\hat{i}, \hat{k}) = (G_{\mathcal{I}}(\hat{z}_i), G_{\mathcal{K}}(\hat{z}_k))$.

2.1 Beyond the Range of Generator

As described earlier, the optimization program (4) implicitly constrains the deblurred image to lie in the range of the generator $G_{\mathcal{I}}$. This may lead to some artifacts in the deblurred images when the generator range does not completely span the set \mathcal{I} . In such case, it makes more sense to not strictly constrain the recovered image to come from the range of the generator, and rather also explore images a bit outside the range. To accomplish this, we propose minimizing the measurement loss of images inside the range exactly as in (3) together with the measurement loss $\|y - i \otimes G_{\mathcal{K}}(z_k)\|^2$ of images not necessarily within the range. The in-range image $G_{\mathcal{I}}(z_i)$ and the out-range image i are then tied together by minimizing an additional penalty term, Range Error(i) := $\|i - G_{\mathcal{I}}(z_i)\|^2$. The idea is to strictly minimize the range error when pretrained generator has effectively learned the image distribution, and afford some slack otherwise. Finally, to guide the search of a best deblurred image beyond the range of the generator, one of the conventional image priors such as total variation measure $\|\cdot\|_{\text{tv}}$ is also introduced. This leads to the following optimization program

$$\operatorname{argmin}_{i, z_i, z_k} \|y - i \otimes G_{\mathcal{K}}(z_k)\|^2 + \tau \|i - G_{\mathcal{I}}(z_i)\|^2 + \zeta \|y - G_{\mathcal{I}}(z_i) \otimes G_{\mathcal{K}}(z_k)\|^2 + \rho \|i\|_{\text{tv}} \quad (5)$$

All of the variables are randomly initialized, and the objective is minimized using gradient step in each of the unknowns, while fixing the others. We take the solution \hat{i} , and $G(\hat{z}_k)$ as the deblurred image, and the recovered blur kernel. We dubbed this approach as *Deep Deblur with Slack* (DDS) and the image deblurred using this approach is referred to as \hat{i}_{DDS} .

3 Experimental Results

In this section, we provide a comprehensive set of experiments to evaluate the performance of *Deep Deblur* and *Deep Deblur with Slack* against iterative and deep learning based baseline methods. We also evaluate performance under increasing noise and large blurs. In all experiments, we use noisy blurred images, generated by convolving images i , and blurs k from their respective test sets and adding 1%¹ Gaussian noise (unless stated otherwise). The choice of free parameters in both algorithms for each dataset are provided in the supplementary material.

3.1 Implementation Details

Datasets: We choose three image datasets. First dataset, SVHN, consists of house number images from Google street view. A total of 531K images, each of dimension $32 \times 32 \times 3$, are available out of which 30K are held out as test set. Second dataset, Shoes [68] consists of 50K RGB examples of shoes, resized to $64 \times 64 \times 3$. We leave 1000 images for testing and use the rest as training set. Third dataset, CelebA, consists of relatively more complex images of celebrity faces. A total of 200K, each center cropped to dimension $64 \times 64 \times 3$, are available out of which 22K are held out as a test set. A motion blur dataset is generated consisting of small to very large blurs of lengths varying between 5 and 28; following strategy given in [9]. We generate 80K blurs out of which 20K is held out as a test set.

Generative Models: We choose VAE as the generative model for SVHN images and motion blurs. For Shoes and CelebA, the generative model $G_{\mathcal{T}}$ is the default deep convolutional generative adversarial network (DCGAN) [28]. Further details on architectures of generative models are provided in the supplementary material.

Baseline Methods: Among the conventional algorithms using engineered priors, we choose dark prior (DP) [25], extreme channel prior (EP) [67], outlier handling (OH) [4], and learned data fitting (DF) [26] based blind deblurring as baseline algorithms. We optimized the parameters of these methods in each experiment to obtain the best possible baseline results. Among driven approaches for deblurring, we choose [13] that trains a convolutional neural network (CNN) in an end-to-end manner, and [18] that trains a neural network (DeblurGAN) in an adversarial manner. Deblurred images from these baseline methods will be referred to as i_{DP} , i_{EP} , i_{OH} , i_{DF} , i_{CNN} and i_{DeGAN} .

3.2 Deblurring Results under Pretrained Generative Priors

The central limiting factor in the *Deep Deblur* performance is the ability of the generator to represent the (original, clean) image to be recovered. As pointed out earlier that often the generators are not fully expressive (cannot generate new representative samples) on a rich/complex image class such as face images compared to a compact/simple image class

¹For an image scaled between 0 and 1, Gaussian noise of 1% translates to Gaussian noise with standard deviation $\sigma = 0.01$ and mean $\mu = 0$.

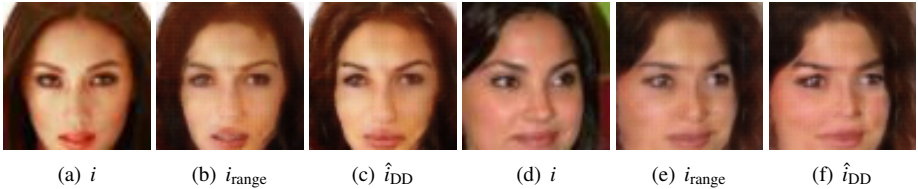


Figure 3: Generator Range Analysis. For each test image i_{test} when blurred, *Deep Deblur* tends to recover corresponding range image i_{range} .

such as numbers. Such a generator mostly cannot *adequately* represent a new image in its range. Since *Deep Deblur* strictly constrains the recovered image to lie in the range of image generator, its performance depends on how well the range of the generator spans the image class. Given an arbitrary test image i_{test} in the set \mathcal{I} , the closest image i_{range} , in the range of the generator, to i_{test} is computed by solving the following optimization program

$$z_{\text{test}} := \underset{z}{\operatorname{argmin}} \|i_{\text{test}} - G_{\mathcal{I}}(z)\|^2, \quad i_{\text{range}} = G_{\mathcal{I}}(z_{\text{test}})$$

We solve the optimization program by running 10,000(6,000) gradient descent steps with a step size of 0.001(0.01) for CelebA(SVHN). Parameters for Shoes are the same as CelebA.

A more expressive generator leads to a better deblurring performance as it can well represent an arbitrary original (clean) image i_{test} leading to a smaller mismatch range error $:= \|i_{\text{test}} - i_{\text{range}}\|$ to the corresponding range image i_{range} .

3.2.1 Impact of Generator Range on Image Deblurring

To judge the proposed deblurring algorithms independently of generator range limitations, we present their deblurring performance on range image i_{range} ; we do this by generating a blurred image $y = i_{\text{range}} \otimes k + n$ from an image i_{range} already in the range of the generator; this implicitly removes the range error as now $i_{\text{test}} = i_{\text{range}}$. We call this range image deblurring, where the deblurred image is obtained using *Deep Deblur*, and is denoted by \hat{i}_{range} . For completeness, we also assess the overall performance of the algorithm by deblurring arbitrary blurred images $y = i_{\text{test}} \otimes k + n$, where i_{test} is not necessarily in the range of the generator. Unlike above, the overall error in this case accounts for the range error as well. We call this arbitrary image deblurring, and specifically the deblurred image is obtained using *Deep Deblur*, and is denoted by \hat{i}_{DD} . Figure 3 shows a qualitative comparison between i_{test} , i_{range} , and \hat{i}_{DD} on CelebA dataset. It is clear that the recovered image \hat{i}_{DD} is a good approximation of the range image, i_{range} , indicating the limitation of the image generative network.

Deep Deblur with Slack mitigates the range error by not strictly constraining the recovered image to lie in the range of the image generator, for details, see Section 2.1. As shown in Figure 4, estimate \hat{i}_{DDS} of true image i_{test} from blurry observations is close to i_{test} instead of i_{range} , thus mitigating the range issue.

3.2.2 Deblurring Results on CelebA, Shoes and SVHN

Qualitative results on CelebA: Figure 4 gives a qualitative comparison between i , i_{range} , \hat{i}_{DD} , \hat{i}_{DDS} , and baseline approaches on CelebA and Shoes dataset. The deblurred images under engineered priors are qualitatively a lot inferior than the deblurred images \hat{i}_{DD} , and



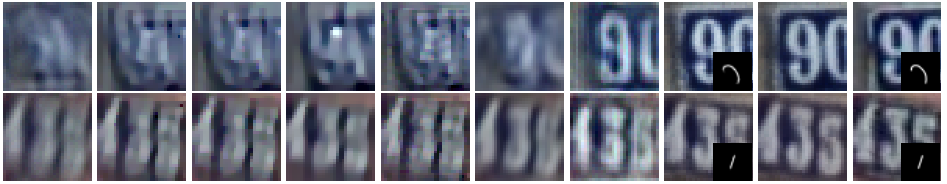
(a) y (b) i_{DP} (c) i_{DF} (d) i_{EP} (e) i_{OH} (f) i_{CNN} (g) i_{DeGAN} (h) \hat{i}_{DD} (i) i_{range} (j) \hat{i}_{DDS} (k) i_{test}
 Figure 4: Image deblurring results on Shoes and CelebA using *Deep Deblur* and *Deep Deblur with Slack*. It can be seen that \hat{i}_{DD} is in close resemblance to i_{range} (closest image in the generator range to the original image), where as \hat{i}_{DDS} is almost exactly i_{test} , thus mitigating the range issue of image generator.



(a) y (b) i_{DP} (c) i_{EP} (d) i_{DF} (e) i_{OH} (f) i_{DeGAN} (g) \hat{i}_{DD} (h) i_{sample}
 Figure 5: Image deblurring results on blurry images generated from samples, i_{sample} , of PGGAN via *Deep Deblur*. Visually appealing images, \hat{i}_{DD} , are recovered, from blurry ones.

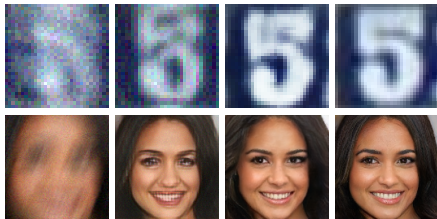
\hat{i}_{DDS} under the proposed generative priors, especially under large blurs. On the other hand, the end-to-end training based approaches CNN, and DeblurGAN perform relatively better, however, the well reputed CNN is still displaying over smoothed images with missing edge details, etc compared to our results \hat{i}_{DDS} . DeblurGAN, though competitive, is outperformed by the proposed *Deep Deblur with Slack* by more than 1.5dB as shown in Table 1. The images \hat{i}_{DD} are sharp and with well defined facial boundaries and markers owing to the fact they strictly come from the range of the generator, however, in doing so these images might end up changing some image features such as expressions, nose, etc. On a close inspection, it becomes clear that how well \hat{i}_{DD} approximates i_{test} roughly depends (see, images specifically in Figure 3) on how close i_{range} is to i_{test} exactly. While as \hat{i}_{DDS} are allowed some leverage, and are not strictly confined to the range of the generator, they tend to agree more closely with the ground truth. We go on further by utilizing pretrained PGGAN [14] in *Deep Deblur* by convolving sampled images with large blurs (30×30); see Figure 5. It has been observed that pre-trained generators struggle at higher resolutions [14], so we restrict our results at 128×128 resolution. In Figure 5, it can be seen that under expressive generative priors our approach exceeds all other baseline methods recovering fine details from extremely blurry images.

Qualitative Results on SVHN: Figure 6 gives qualitative comparison between proposed and baseline methods on SVHN dataset. Here the deblurring under classical priors again clearly under performs compared to the proposed image deblurring results \hat{i}_{DD} . CNN also continues to be inferior, and the DeblurGAN also shows artifacts. We do not include the



(a) y (b) i_{DP} (c) i_{OH} (d) i_{DF} (e) i_{EP} (f) i_{CNN} (g) i_{DGAN} (h) \hat{i}_{DD} (i) \hat{i}_{range} (j) \hat{i}_{test}

Figure 6: Image deblurring results on SVHN images using *Deep Deblur*. It can be seen that due to the simplicity of these images, \hat{i}_{DD} is a visually a very good estimate of \hat{i}_{test} , due to the close proximity between \hat{i}_{range} and \hat{i}_{test} .



(a) y (b) \hat{i}_{DeGAN}^* (c) \hat{i}_{DD} (d) \hat{i}_{test}

Figure 7: Visual Comparison of DeblurGAN (\hat{i}_{DeGAN}^*) trained on 1-10% noise with *Deep Deblur* on noisy images from SVHN (top row) and samples from PGGAN (bottom row).



Figure 8: Large Blurs. Under large blurs, proposed *Deep Deblur with Slack*, shows excellent deblurring results.

results \hat{i}_{DDS} in these comparison as \hat{i}_{DD} already comprehensively outperform the other techniques on this dataset. The convincing results \hat{i}_{DD} are a manifestation of the fact that unlike the relatively complex CelebA and Shoes datasets, the simpler image dataset SVHN is effectively spanned by the range of the image generator.

Quantitative Results: Quantitative results for CelebA, Shoes² and SVHN using peak-signal-to-noise ratio (PSNR) and structural-similarity index (SSIM) [53], averaged over 80 respective test set images, are given in Table 1. On CelebA and Shoes, the results clearly show a better performance of *Deep Deblur with Slack*, on average, compared to all baseline methods. On SVHN, the results show that *Deep Deblur* outperforms all competitors. The fact that *Deep Deblur* performs more convincingly on SVHN is explained by observing that the range images \hat{i}_{range} in SVHN are quantitatively much better compared to range images of CelebA and Shoes.

3.2.3 Robustness against Noise and Large Blurs

Robustness against Noise: Figure 9 gives a quantitative comparison of the deblurring obtained via *Deep Deblur* (the free parameters λ , γ and random restarts in the algorithm are fixed as before), and baseline methods CNN, DeblurGAN (trained on fixed 1% noise level and on varying 1-10% noise levels) in the presence of Gaussian noise. We also include the performance of deblurred range images \hat{i}_{range} , introduced in Section 3.2, as a benchmark.

²For qualitative results, see supplementary material.

Method		\hat{i}_{EP}	\hat{i}_{DF}	\hat{i}_{OH}	\hat{i}_{DP}	\hat{i}_{DeGAN}	\hat{i}_{CNN}	\hat{i}_{DD}	\hat{i}_{DDS}	\hat{i}_{range}
SVHN	PSNR	20.35	20.64	20.82	20.91	15.79	21.24	24.47	-	30.13
	SSIM	0.55	0.60	0.58	0.58	0.54	0.63	0.80	-	0.89
Shoes	PSNR	18.33	17.79	19.04	18.45	21.84	24.76	21.20	26.98	23.93
	SSIM	0.73	0.73	0.76	0.74	0.85	0.89	0.83	0.93	0.87
CelebA	PSNR	17.80	20.00	20.71	21.09	24.01	23.75	21.11	26.60	25.49
	SSIM	0.70	0.79	0.81	0.79	0.88	0.87	0.80	0.93	0.91

Table 1: Quantitative comparison of proposed approach with baseline methods on CelebA, SVHN, and Shoes dataset. Table shows average PSNR and SSIM on 80 random images from respective test sets.

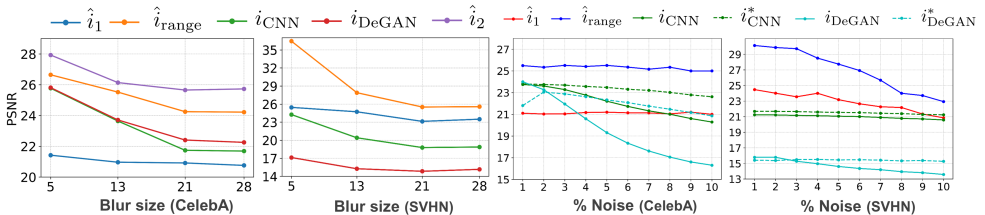


Figure 9: Blur Size and Noise Analysis. Comparative performance of proposed methods, on CelebA and SVHN dataset, against baseline techniques, as blur length and noise level increases.

Conventional prior based approaches are not included as their performance substantially suffers on noise compared to other approaches. On the vertical axis, we plot the PSNR and on the horizontal axis, we vary the noise strength from 1 to 10%. In general, the quality of deblurred range images (expressible by the generators) \hat{i}_{range} under generative priors surpasses other algorithms on both CelebA, and SVHN. This in a way manifests that under expressive generative priors, the performance of our approach is far superior. The quality of deblurred images \hat{i}_{DD} under generative priors with arbitrary (not necessarily in the range of the generator) input images is the second best on SVHN, however, it under performs on the CelebA dataset; the most convincing explanation of this performance deficit is the range error (not as expressive generator) on the relatively complex/rich images of CelebA. The end-to-end approaches trained on fixed 1% noise level display a rapid deterioration on other noise levels. Comparatively, the ones trained on 1-10% noise level, expectedly, show a more graceful performance. Qualitative results under heavy noise are depicted in Figure 7. Our deblurred image \hat{i}_{DD} visually agrees better with i_{test} than other methods.

Robustness against Large Blurs: Figure 8 shows the deblurred images obtained from a very blurry face image. The deblurred image \hat{i}_{DDS} using *Deep Deblur with Slack* is able to recover the true face from a completely unrecognizable face. The classical baseline algorithms totally succumb to such large blurs. The quantitative comparison against end-to-end neural network based methods CNN, and DeblurGAN is given in Figure 9. We plot the blur size against the average PSNR for both Shoes, and CelebA datasets. On both datasets, deblurred images \hat{i}_{DDS} convincingly outperforms all other techniques. For comparison, we also add the performance of \hat{i}_{range} . Excellent deblurring under large blurs can also be seen in Figure 5 for PGGAN. To summarize, the end-to-end approaches begin to lag a lot behind our proposed algorithms when the blur size increases. This is owing to the firm control induced by the powerful generative priors on the deblurring process in our newly proposed algorithms.

4 Conclusion

This paper proposes a novel framework for blind image deblurring that uses deep generative networks as priors rather than in a conventional end-to-end manner. We report convincing deblurring results under the generative priors in comparison to the existing methods. A thorough discussion on the possible limitations of this approach on more complex images is presented along with an effective remedy to address these shortcomings. Our main contribution lies in introducing pretrained generative model in solving blind deconvolution. Introducing more expressive generative models with new novel architectures would improve the performance. We leave these exciting directions for future work.

References

- [1] Shahrukh Athar, Evgeny Burnaev, and Victor Lempitsky. Latent convolutional models. 2018.
- [2] Ashish Bora, Ajil Jalal, Eric Price, and Alexandros G Dimakis. Compressed sensing using generative models. *arXiv preprint arXiv:1703.03208*, 2017.
- [3] Giacomo Boracchi, Alessandro Foi, et al. Modeling the performance of image restoration from motion blur. *IEEE Trans. Image Processing*, 21(8):3502–3517, 2012.
- [4] Jian-Feng Cai, Hui Ji, Chaoqiang Liu, and Zuowei Shen. Blind motion deblurring from a single image using sparse approximation. In *Computer Vision and Pattern Recognition, 2009. CVPR 2009. IEEE Conference on*, pages 104–111. IEEE, 2009.
- [5] Patrizio Campisi and Karen Egiazarian. *Blind image deconvolution: theory and applications*. CRC press, 2016.
- [6] Tony F Chan and Chiu-Kwong Wong. Total variation blind deconvolution. *IEEE transactions on Image Processing*, 7(3):370–375, 1998.
- [7] Jiangxin Dong, Jinshan Pan, Zhixun Su, and Ming-Hsuan Yang. Blind image deblurring with outlier handling. In *IEEE International Conference on Computer Vision (ICCV)*, pages 2478–2486, 2017.
- [8] Rob Fergus, Barun Singh, Aaron Hertzmann, Sam T Roweis, and William T Freeman. Removing camera shake from a single photograph. In *ACM transactions on graphics (TOG)*, volume 25, pages 787–794. ACM, 2006.
- [9] Yossi Gandelsman, Assaf Shocher, and Michal Irani. "double-dip": Unsupervised image decomposition via coupled deep-image-priors. *arXiv preprint arXiv:1812.00467*, 2018.
- [10] Ian Goodfellow, Jean Pouget-Abadie, Mehdi Mirza, Bing Xu, David Warde-Farley, Sherjil Ozair, Aaron Courville, and Yoshua Bengio. Generative adversarial nets. In *Advances in neural information processing systems*, pages 2672–2680, 2014.
- [11] Paul Hand and Vladislav Voroninski. Global guarantees for enforcing deep generative priors by empirical risk. *arXiv preprint arXiv:1705.07576*, 2017.

- [12] Paul Hand, Oscar Leong, and Vlad Voroninski. Phase retrieval under a generative prior. In *Advances in Neural Information Processing Systems*, pages 9154–9164, 2018.
- [13] Michal Hradiš, Jan Kotera, Pavel Zemčík, and Filip Šroubek. Convolutional neural networks for direct text deblurring. In *Proceedings of BMVC*, volume 10, 2015.
- [14] Zhe Hu, Jia-Bin Huang, and Ming-Hsuan Yang. Single image deblurring with adaptive dictionary learning. In *Image Processing (ICIP), 2010 17th IEEE International Conference on*, pages 1169–1172. IEEE, 2010.
- [15] Tero Karras, Timo Aila, Samuli Laine, and Jaakko Lehtinen. Progressive growing of gans for improved quality, stability, and variation. *arXiv preprint arXiv:1710.10196*, 2017.
- [16] Diederik P Kingma and Max Welling. Auto-encoding variational bayes. *arXiv preprint arXiv:1312.6114*, 2013.
- [17] Deepa Kundur and Dimitrios Hatzinakos. Blind image deconvolution. *IEEE signal processing magazine*, 13(3):43–64, 1996.
- [18] Orest Kupyn, Volodymyr Budzan, Mykola Mykhailych, Dmytro Mishkin, and Jiri Matas. Deblurgan: Blind motion deblurring using conditional adversarial networks. *arXiv preprint arXiv:1711.07064*, 2017.
- [19] Anat Levin, Yair Weiss, Fredo Durand, and William T Freeman. Understanding and evaluating blind deconvolution algorithms. In *Computer Vision and Pattern Recognition, 2009. CVPR 2009. IEEE Conference on*, pages 1964–1971. IEEE, 2009.
- [20] Lerenhan Li, Jinshan Pan, Wei-Sheng Lai, Changxin Gao, Nong Sang, and Ming-Hsuan Yang. Learning a discriminative prior for blind image deblurring. In *Proceedings of the IEEE Conference on Computer Vision and Pattern Recognition*, pages 6616–6625, 2018.
- [21] Alice Lucas, Michael Iliadis, Rafael Molina, and Aggelos K Katsaggelos. Using deep neural networks for inverse problems in imaging: beyond analytical methods. *IEEE Signal Processing Magazine*, 35(1):20–36, 2018.
- [22] Seungjun Nah, Tae Hyun Kim, and Kyoung Mu Lee. Deep multi-scale convolutional neural network for dynamic scene deblurring. *arXiv preprint arXiv:1612.02177*, 2016.
- [23] TM Nimisha, Akash Kumar Singh, and AN Rajagopalan. Blur-invariant deep learning for blind-deblurring. In *Proceedings of the IEEE Conference on Computer Vision and Pattern Recognition*, pages 4752–4760, 2017.
- [24] Jinshan Pan, Risheng Liu, Zhixun Su, and Guili Liu. Motion blur kernel estimation via salient edges and low rank prior. In *Multimedia and Expo (ICME), 2014 IEEE International Conference on*, pages 1–6. IEEE, 2014.
- [25] Jinshan Pan, Deqing Sun, Hanspeter Pfister, and Ming-Hsuan Yang. Blind image deblurring using dark channel prior. In *Proceedings of the IEEE Conference on Computer Vision and Pattern Recognition*, pages 1628–1636, 2016.

- [26] Jinshan Pan, Jiangxin Dong, Yu-Wing Tai, Zhixun Su, and Ming-Hsuan Yang. Learning discriminative data fitting functions for blind image deblurring. In *ICCV*, pages 1077–1085, 2017.
- [27] Wenqi Ren, Xiaochun Cao, Jinshan Pan, Xiaojie Guo, Wangmeng Zuo, and Ming-Hsuan Yang. Image deblurring via enhanced low-rank prior. *IEEE Transactions on Image Processing*, 25(7):3426–3437, 2016.
- [28] Tim Salimans, Ian Goodfellow, Wojciech Zaremba, Vicki Cheung, Alec Radford, and Xi Chen. Improved techniques for training gans. In *Advances in Neural Information Processing Systems*, pages 2234–2242, 2016.
- [29] Christian J Schuler, Michael Hirsch, Stefan Harmeling, and Bernhard Schölkopf. Learning to deblur. *IEEE transactions on pattern analysis and machine intelligence*, 38(7):1439–1451, 2016.
- [30] Viraj Shah and Chinmay Hegde. Solving linear inverse problems using gan priors: An algorithm with provable guarantees. *arXiv preprint arXiv:1802.08406*, 2018.
- [31] Fahad Shamshad and Ali Ahmed. Robust compressive phase retrieval via deep generative priors. *arXiv preprint arXiv:1808.05854*, 2018.
- [32] Fahad Shamshad, Farwa Abbas, and Ali Ahmed. Deep ptych: Subsampled fourier ptychography using generative priors. *arXiv preprint arXiv:1812.11065*, 2018.
- [33] Zhou Wang, Alan C Bovik, Hamid R Sheikh, and Eero P Simoncelli. Image quality assessment: from error visibility to structural similarity. *IEEE transactions on image processing*, 13(4):600–612, 2004.
- [34] Li Xu, Cewu Lu, Yi Xu, and Jiaya Jia. Image smoothing via l0 gradient minimization. In *ACM Transactions on Graphics (TOG)*, volume 30, page 174. ACM, 2011.
- [35] Xiangyu Xu, Deqing Sun, Jinshan Pan, Yujin Zhang, Hanspeter Pfister, and Ming-Hsuan Yang. Learning to super-resolve blurry face and text images. In *Proceedings of the IEEE Conference on Computer Vision and Pattern Recognition*, pages 251–260, 2017.
- [36] Yanyang Yan, Wenqi Ren, Yuanfang Guo, Rui Wang, and Xiaochun Cao. Image deblurring via extreme channels prior. In *Proceedings of the IEEE Conference on Computer Vision and Pattern Recognition*, pages 4003–4011, 2017.
- [37] Raymond A Yeh, Chen Chen, Teck Yian Lim, Alexander G Schwing, Mark Hasegawa-Johnson, and Minh N Do. Semantic image inpainting with deep generative models. In *Proceedings of the IEEE Conference on Computer Vision and Pattern Recognition*, pages 5485–5493, 2017.
- [38] Aron Yu and Kristen Grauman. Fine-grained visual comparisons with local learning. In *Proceedings of the IEEE Conference on Computer Vision and Pattern Recognition*, pages 192–199, 2014.
- [39] Haichao Zhang, Jianchao Yang, Yanning Zhang, and Thomas S Huang. Sparse representation based blind image deblurring. In *Multimedia and Expo (ICME), 2011 IEEE International Conference on*, pages 1–6. IEEE, 2011.